

Adaptation of Weakly Supervised Localization in Histopathology by Debiasing Predictions

Alexis Guichemerre¹✉, Banafsheh Karimian¹, Soufiane Belharbi¹, Natacha Gillet¹, Nicolas Thome², Pourya Shamsolmoali³, Mohammadhadi Shateri¹, Luke McCaffrey⁴, and Eric Granger¹

¹ ÉTS Montréal, Montreal, Canada

² Sorbonne Université, Paris, France

³ University of York, York, United Kingdom

⁴ McGill University, Montreal, Canada

alexis.guichemerre.1@ens.etsmtl.ca

Abstract. Weakly Supervised Object Localization (WSOL) models enable joint classification and region-of-interest localization in histology images using only image-class supervision. When deployed in a target domain, distributions shift remains a major cause of performance degradation, especially when applied on new organs or institutions with different staining protocols and scanner characteristics. Under stronger cross-domain shifts, WSOL predictions can become biased toward dominant classes, producing highly skewed pseudo-label distributions in the target domain. Source-Free (Unsupervised) Domain Adaptation (SFDA) methods are commonly employed to address domain shift. However, because they rely on self-training, the initial bias is reinforced over training iterations, degrading both classification and localization tasks. We identify this amplification of prediction bias as a primary obstacle to the SFDA of WSOL models in histopathology.

This paper introduces **SFDA-DeP**, a method inspired by machine unlearning that formulates SFDA as an iterative process of identifying and correcting prediction bias. It periodically identifies target images from over-predicted classes and selectively reduces the predictive confidence for uncertain (high entropy) images, while preserving confident predictions. This process reduces the drift of decision boundaries and bias toward dominant classes. A jointly optimized pixel-level classifier further restores discriminative localization features under distribution shift. Extensive experiments on cross-organ and -center histopathology benchmarks (GlaS, CAMELYON16, CAMELYON17) with several WSOL models show that SFDA-DeP consistently improves classification and localization over state-of-the-art SFDA baselines. Code: anonymous.4open.science/r/SFDA-DeP-1797/

Keywords: Weakly Supervised Object Localization · Source-Free Domain Adaptation · Machine Unlearning · Histopathology.

1 Introduction

Computer-aided diagnostic systems based on deep learning are increasingly explored in digital pathology to support large-scale cancer screening and grad-

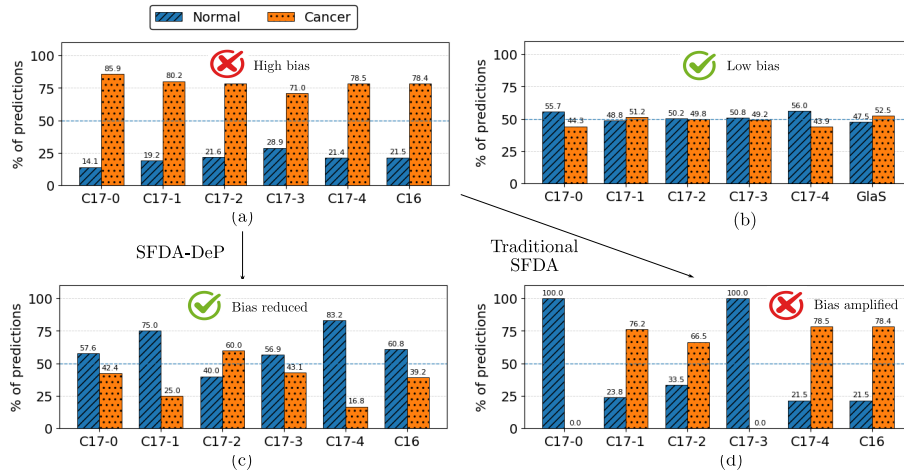


Fig. 1. (a) Source-only inference shows a strong predictive bias toward the cancer class when transferring from GlaS (source) to CAMELYON16 and CAMELYON17 (target). (b) Using CAMELYON16 as source yields more balanced predictions across targets (CAMELYON17 and GlaS). (c) SFDA-DeP is shown to reduce predictive bias across centers. (d) In contrast, traditional SFDA, such as SFDA-DE amplifies bias, often collapsing to a dominant class. (The dashed line indicates the ideal 50% predictive balance for these datasets.)

ing [11,14,20]. However, most state-of-the-art approaches rely on densely annotated datasets, where pixel-level annotations of tumor regions remain labor-intensive and require expert pathologists [10,11,20]. Deep WSOL models mitigate this limitation by jointly predicting the image-level diagnosis and highlighting discriminative tissue regions after training on data with only image-class labels [18]. Domain shifts in histopathology are commonly attributed to variations in staining protocols, scanner characteristics, tissue processing, and organ-specific tissue architecture [4,10,11]. However, empirical analysis as in Fig. 1 reveals that performance degradation in WSOL is particularly pronounced for shifts across organs and dataset-scale imbalance [10,11]. When a WSOL model trained on a small source dataset (possibly from a different organ) is deployed on a larger target dataset collected at another center, both classification accuracy and spatial localization quality degrade [10]. Conversely, models trained on large-scale datasets exhibit more stable cross-domain behavior. This transfer pattern suggests that the failure of WSOL under critical domain shift extends beyond low-level appearance changes and is strongly influenced by semantic and distributional mismatch. In digital pathology, this spatial drift directly compromises interpretability and clinical reliability [10].

SFDA provides a practical framework for cross-center and cross-organ deployment by adapting a source-trained model using only unlabeled target data [22,31]. Most existing SFDA approaches rely on pseudo-labeling or clustering mechanisms [19] that implicitly assume that the source classifier remains sufficiently

discriminative [21] on the target domain to reliably separate target samples by predicted class [10,17]. Under severe shift such as cross-organ and distributional shifts in histopathology, this assumption often breaks down [10]. The source model may become bias by over-predicting a subset of classes while under-representing others, leading to highly skewed distribution as in Fig. 1. When applied to biased predictions, SFDA performance is limited, as these methods tend to reinforce existing class asymmetries rather than correct them, as the feature space itself has been shaped by the source decision boundary [10]. In WSOL setting, this classification-level bias further propagates to spatial cues, causing the model to learn inconsistent and unreliable localization patterns.

To address this limitation, a SFDA method for debiasing predictions (SFDA-DeP) is introduced to mitigate prediction bias under domain shift [10]. Over-predicted classes can bias the adaptation process by disproportionately influencing target sample assignments. Inspired by machine unlearning approaches [25,28], our proposed method reduce the contribution of uncertain image samples from dominant classes, identified through normalized entropy. By increasing uncertainty for these samples, the deep WSOL model avoids reinforcing biased assignments during boundary refinement. Meanwhile, stable samples are retained to support consistent and transferable class separation. To enhance spatial discrimination under domain shift, a lightweight pixel-level head is jointly optimized for foreground/background priors derived from class activation maps (CAMs), improving foreground-background separation after adaptation.

2 Related Work

(a) Weakly Supervised Object Localization: WSOL models infer spatial evidence from image-level supervision, through class activation mapping (CAM) mechanisms [3,9,13] where localization maps are directly induced by classifier responses. Representative WSOL approaches can broadly be categorized into bottom-up (forward-pass information) and top-down strategies (exploit both forward and backward information) [20]. Representative bottom-up methods include DeepMIL [12], where instance-level attention weights highlight relevant patches, and transformer-based models such as SAT [26], where token interactions refine class-specific attention maps. In histopathology, approaches such as NEGEV [2] and PixelCAM [11] introduce additional spatial refinement mechanisms to improve pixel-level attribution. Robustness of WSOL models under cross-domain conditions remains relatively underexplored in histopathology, and few analyses report significant performance degradation when models are transferred across organs or centers on both tasks [10,11].

(b) Source-Free Unsupervised Domain Adaptation: SFDA addresses domain shift by adapting a pretrained source model to a new target domain using only unlabeled target data, thereby avoiding additional annotation cost and eliminating the need to access source data. Most approaches rely on pseudo-label refinement via clustering or predictions [8,16]. These strategies implicitly assume that the source classifier provides sufficiently reliable predictions on tar-

get samples to guide adaptation [5,17]. In practice, this assumption depends on the stability of source predictions under domain shift. Under severe domain shift, especially cross-organ shifts in histopathology, this assumption frequently fails [10] as the source model produces skewed pseudo-label distributions on the target domain [10]. When optimization proceeds using these biased assignments, adaptation primarily reinforces already confident predictions, limiting the model’s ability to recover underrepresented classes [10]. As a result, class imbalance persists throughout training rather than being progressively corrected, degrading the performance of classification and localization tasks.

(c) Machine Unlearning: Recent work explores removing non-transferable or undesirable knowledge from pretrained models, often motivated by privacy constraints or partial-set adaptation [25]. These methods typically operate at the dataset or class level, suppressing specific representations learned from the source domain [1,15,25,28]. In contrast, our objective is not to erase classes or source knowledge, but to correct biased target predictions under domain shift. Rather than removing data, we selectively attenuate uncertain pseudo-label assignments to reshape the decision boundary during target adaptation, while preserving reliable target information.

3 Proposed SFDA-DeP Method

Notations. Let us denote by $\mathbb{T} = \{x_i\}_{i=1}^N$ an unlabeled target training set composed of N images $x_i : \Omega \subset \mathbb{R}^2$, where Ω is a discrete image domain. We consider a classifier $f(x) \in [0, 1]^K$ that was pre-trained on source data $\mathbb{S} = \{(x, y)_i\}_{i=1}^M$ labeled only with image classes $y \in \{1, \dots, K\}$ where K is the total number of classes. The feature extractor of f is denoted by $g(x) = Z \in \mathbb{R}^{|\Omega| \times d}$, with d as feature dimension. We refer by $z_p \in \mathbb{R}^d$ to the pixel embedding at location point p in Ω . Only the image classifier f is pre-trained on the source dataset that is no longer accessible during adaptation over target data.

Class prediction bias and its correction. Over the target set \mathbb{T} , and without any adaptation, the pre-trained model f over the source data can yield highly imbalanced predictions where some classes are predicted more frequently. This is mainly caused by the large domain shift between source and target data. Such class imbalance can be detected over the target set without any supervision by simply considering the class prediction frequency as illustrated in Fig.1(a). For simplicity, we denote by $\mathbb{B} = \{x \in \mathbb{T} : \hat{y}(x) \in \mathcal{B}\}$, where $\hat{y}(x) = \arg \max_c p_{\phi_{trg}}(y = c | x)$, the set containing the samples predicted as one of the dominant classes \mathcal{B} . Our method aims to move the classifier f class-boundaries around dominant classes, allowing minority classes to be predicted more often. To this end, and inspired by the machine unlearning field [1,15,25,28], we consider two sets that can leverage some of the reliable predictions and also help move class boundaries. In a parallel analogy to machine unlearning, we aim for the classifier to forget the old class boundaries and establish new ones that lead to balanced class prediction.

We consider a *forget set* $\mathbb{B}_f \subset \mathbb{B}$ which contains the top- ρ most uncertain samples from dominant classes located near the class-boundaries defined as:

$$\mathbb{B}_f = \text{top}_\rho(\mathbb{B}, H(x)), \quad (1)$$

where $H(x)$ denote the prediction uncertainty using normalized entropy.

Our new adaptation aims for the model to forget the assigned dominant classes for these samples and discourages reinforcement of biased assignments (obtaining balanced prediction) and promotes boundary correction. We refer to all the remaining samples of the target data $\mathbb{B}_r = \mathbb{T} - \mathbb{B}_f$ as *retain set*. It contains certain samples which can be fitted to the model in a self-supervised way. We defined the retain loss as a standard cross-entropy,

$$\mathcal{L}_{\text{retain}} = \mathbb{E}_{x_i \in \mathbb{B}_r} \left[-\log(p_i(\hat{y})) \right], \quad (2)$$

where $\hat{y}(x) = \arg \max_c p_{\phi_{\text{trg}}}(y = c | x)$ and its minimization allows the model to continue predicting the same sample pseudo-label \hat{y} . However, for the forget set, we aim for the model to stop predicting the sample predicted class. Therefore, we consider maximizing its standard cross-entropy, which is equivalent to minimizing negative cross-entropy:

$$\mathcal{L}_{\text{forget}} = \mathbb{E}_{x_i \in \mathbb{B}_f} \left[-\log(1 - p_i(\hat{y})) \right], \quad (3)$$

Minimizing Eq.3 pushes the model to refrain from predicting the same dominant class \hat{y} for samples in the forget set, and assign a new class. Optimizing both losses (Eq.2, 3) aims to redefine the class-boundaries of the model over the target data by leveraging the most reliable samples, and samples near the boundaries. We note that the forget and retain sets can be defined once during the adaptation. However, to avoid overfitting incorrect pseudo-labels, and account for the change in class-boundaries, we consider rebuilding both sets using the current model every m epochs.

Localization supervision : Accurate class-prediction allows the adapted model for a better localization. However, due to a large domain shift, target regions of interest (ROI) could be visually very different from the source data, making localization even more difficult. To maintain discriminative pixel-level representations during adaptation, we consider a classifier h at the pixel-embedding level. It allows directly classifying a pixel into ROI (foreground) or background. The locations of the known pseudo-labels are encoded in Ω' . To this end, we define over each target sample a mask of pixel-wise partial pseudo-labels denoted $\mathbf{Y} \in \{0, 1\}^{|\Omega| \times 2}$, $\mathbf{Y}_p \in \{0, 1\}^2$ at location p with value 0 for background, 1 for foreground. For each predicted class k , we select only the top- ρ_{loc} fraction of samples with the lowest entropy and denote their union by D_{loc} . The supervision is performed by extracting CAM from the source model. The pixel-classifier is trained using those pseudo-labels using standard binary cross-entropy loss.

$$\mathcal{L}_{\text{loc}} = -(1 - \mathbf{Y}_p) \log(h(z_p)_0) - \mathbf{Y}_p \log(h(z_p)_1), \quad p \in \Omega'. \quad (4)$$

Our total adaptation loss is composed of three terms optimized jointly. The first two terms are used to steer the model from class prediction bias while maintaining reliable predictions. The last term aims at anchoring localization to avoid drifting during adaptation. The total loss is formulated as follows :

$$\mathcal{L} = \lambda_{\text{retain}}\mathcal{L}_{\text{retain}} + \lambda_{\text{forget}}\mathcal{L}_{\text{forget}} + \lambda_{\text{loc}}\mathcal{L}_{\text{loc}}. \quad (5)$$

4 Results and Discussion

4.1 Experimental Methodology:

Datasets: We evaluate our approach on three publicly available histopathology benchmarks that enable both cross-organ and cross-center domain shifts. **GlaS** provides gland-level annotations for colon cancer [23,20], while **CAMELYON16** and **CAMELYON17** focuses on breast lymph-node metastasis detection [7,20,29]. We use **CAMELYON17** [29] and construct a WSOL-compliant patch-level benchmark that supports classification and localization evaluation with the provided tumor segmentation masks. Following [20], we perform a *center-wise* WSI split: for each medical center, we select *per class* 8/2/2 WSIs (tumor and normal) for train/validation/test, yielding five target domains (C17-0 to C17-4) that simulate cross-center shifts. Concretely, we sample tissue patches with sufficient foreground to avoid trivial patches and ensure meaningful localization [20]. Table 1 reports the resulting number of patches per split. Counts vary across centers due to differences in tumor area annotated. Specifically, we extract patches containing sufficient foreground tumor regions to avoid trivial foreground samples, ensuring meaningful localization supervision [20].

Table 1. Dataset splits used in our experiments, showing the number of patches per split for each dataset and center.

	GlaS	C16	C17-0	C17-1	C17-2	C17-3	C17-4
Train	67	24348	634	1066	498	816	940
Val (CL)	18	8850	144	38	110	102	146
Val (PxAP)	6	10	10	10	10	10	10
Test	80	15664	262	172	448	376	298

Backbone: For CNN, we use ResNet-50 [11,20], while transformer-based models rely on DeiT-Tiny [6,11]. Results are reported with three WSOL methods: **SAT** [26], **PixelCAM** [11], and **DeepMIL** [12]. For fair comparison, source pretraining and hyperparameters follow [10,11]. This source model is used as the initialization for the adaptation stage.

SFDA-DeP hyperparameters:

The retain and forget loss weights are set as $\lambda_{\text{retain}}, \lambda_{\text{forget}} \in \{0.2, 0.5, 1.0, 2.0\}$. The localization loss weight is chosen from $\lambda_{\text{loc}} \in \{0.5, 1.0, 5.0\}$. The learning

Table 2. Localization (PxAP) and classification (CL) accuracy. Results shown for G1aS \rightarrow C16, C17-0, C17-1, C17-2, C17-3, C17-4.

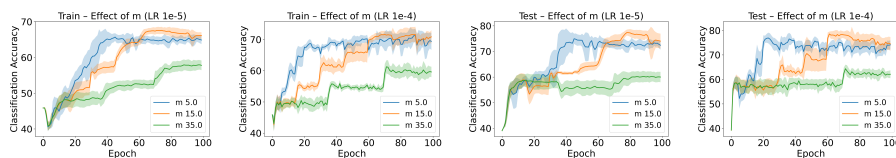
Methods		C16		C17-0		C17-1		C17-2		C17-3		C17-4		Avg	
		PxAP	CL												
PixelCAM (MMDL25)	Source only	37.9	51.8	37.2	41.2	27.2	58.7	44.9	64.9	43.1	39.1	31.1	39.9	36.9	49.3
	SFDA-DE (CVPR'22)	<u>37.9</u>	51.8	14.5	50.0	36.7	<u>65.7</u>	28.9	<u>70.5</u>	18.9	<u>49.9</u>	31.1	39.9	28.0	54.6
	CDCL (TMM'22)	<u>37.9</u>	51.8	25.3	50.0	21.2	59.3	25.5	69.9	19.3	<u>49.9</u>	22.6	40.9	25.3	53.6
	ERL (ICLR'23)	29.9	<u>59.7</u>	13.2	<u>59.5</u>	14.6	67.4	43.0	69.4	19.3	<u>49.9</u>	<u>32.4</u>	54.0	25.4	<u>59.9</u>
	RGV (CVPR'25)	30.7	52.9	<u>31.0</u>	50.0	<u>29.4</u>	53.5	<u>44.9</u>	64.9	<u>40.2</u>	<u>49.9</u>	32.2	41.6	<u>34.7</u>	52.1
	Ours	49.5	67.2	49.9	86.2	27.2	41.3	50.2	76.1	53.8	80.6	33.9	<u>51.3</u>	44.1	67.1
SAT (ICCV'23)	Source only	24.9	54.0	16.8	54.9	17.4	50.6	28.8	52.5	21.0	53.2	18.9	47.3	21.3	52.1
	SFDA-DE (CVPR'22)	26.8	62.9	14.9	76.3	17.8	61.0	32.8	69.9	14.1	76.3	22.9	<u>65.8</u>	21.6	68.7
	CDCL (TMM'22)	32.3	<u>66.6</u>	14.4	72.5	<u>18.3</u>	56.4	<u>33.5</u>	<u>72.8</u>	16.1	<u>77.4</u>	17.4	55.4	22.0	66.9
	ERL (ICLR'23)	<u>32.6</u>	<u>66.6</u>	14.4	69.8	15.1	55.2	32.2	73.2	<u>22.4</u>	79.3	16.3	69.1	<u>22.2</u>	<u>68.9</u>
	RGV (CVPR'25)	24.9	54.0	<u>16.8</u>	54.9	17.4	50.6	28.0	52.4	20.9	49.9	18.9	48.3	21.2	51.7
	Ours	36.4	66.8	24.9	<u>74.8</u>	26.9	<u>57.6</u>	43.7	73.2	27.8	<u>77.4</u>	<u>22.3</u>	65.4	30.3	69.2
DeepMIL (ICML'18)	Source only	24.1	54.0	14.1	45.0	18.4	56.4	30.5	61.8	18.1	38.8	19.1	42.6	20.9	49.8
	SFDA-DE (CVPR'22)	21.6	51.9	14.5	<u>50.0</u>	<u>18.4</u>	56.4	<u>32.5</u>	<u>72.5</u>	16.6	49.9	19.1	42.6	20.5	53.9
	CDCL (TMM'22)	24.0	<u>54.1</u>	<u>27.2</u>	<u>50.0</u>	<u>18.4</u>	56.4	27.8	72.3	<u>37.6</u>	49.9	<u>28.6</u>	<u>50.0</u>	<u>27.3</u>	55.5
	ERL (ICLR'23)	<u>25.7</u>	53.8	12.1	<u>50.0</u>	10.9	65.1	19.4	71.8	16.1	<u>59.3</u>	12.9	46.6	16.2	<u>57.8</u>
	RGV (CVPR'25)	24.7	52.9	27.1	<u>50.0</u>	<u>18.4</u>	<u>56.9</u>	31.1	62.1	21.0	49.9	21.7	43.9	24.0	52.6
	Ours	53.5	72.1	34.0	82.8	38.8	54.1	45.4	79.2	37.7	77.9	34.5	74.5	40.7	73.4

rate is selected from $\{10^{-5}, 10^{-4}, 10^{-3}\}$. The forgetting ratio is explored within $\rho \in \{5\%, 15\%, 25\%\}$.

Implementation details: For source pretraining, we adopt the same setup as in [20].

We compare our method against representative source-free domain adaptation (SFDA) approaches. We evaluate SFDA-DE [5], CDCL [24], ERL [30], and RGV [27]. For fair comparison, optimization parameters (learning rate, decay step size, and decay factor γ , loss weights) are kept consistent across methods.

Impact on classification and localization. Table 2 shows that SFDA-DeP improves WSOL adaptation on most target domains and across architectures, with the largest gains observed where several SFDA baselines remain around 50% CL and exhibit strong dominant-class prediction bias. For PixelCAM, SFDA-DeP reaches **44.1 PxAP** / **67.1 CL** on average, yielding significant improvements over SFDA-DE (+16.1 PxAP and +12.5 CL). Gains are particularly pronounced on CAMELYON17 centers where several baselines remain around 50% CL (e.g., C17-0 and C17-3), while SFDA-DeP improves accuracy (up to 86.2% CL on C17-0). For DeepMIL, SFDA-DeP improves both tasks, reaching **40.7 PxAP** and **73.4 CL** on average (+20.2 PxAP and +19.5 CL vs. SFDA-DE). For the transformer-based SAT,

**Fig. 2.** Effect of dynamic resampling frequency during adaptation with PixelCAM.

improvements are mainly on localization (**30.3 PxAP** average), while classification is relatively stable across methods, leading to smaller gains in **CL**.

Impact of resampling \mathbb{B}_r and Localization supervision. Ablations further indicate that dynamic resampling of \mathbb{B}_r and the pixel-level localization loss are key components of SFDA-DeP. As shown in Table 2 and Fig. 2 and 3, frequent reassignment prevents early incorrect forgetting decisions from becoming irreversible, acting as an iterative correction mechanism. Fig. 3 additionally shows that introducing pixel-level supervision boosts PxAP (e.g., PixelCAM). Qualitative CAMs (Fig. 4) support this observation: SFDA-DeP yields more coherent activations concentrated on tumor tissue, with reduced responses on background regions, whereas SFDA baselines often highlight spurious areas under strong shift.

5 Conclusion

This paper introduces SFDA-DeP, a SFDA method that debiases predictions for WSOL in histopathology that explicitly mitigates dominant class prediction bias under significant cross-domain shifts. SFDA-DeP considers adaptation as an iterative process inspired by machine unlearning: uncertain image samples from over-predicted classes are selectively penalized, while other samples are retained to refine the decision-boundary. A jointly pixel-level head optimized with CAM-consistency is also employed to restore discriminative localization under domain shift, improving foreground/background separation after adaptation. In our experimental validation with cross-organ (GlaS \rightarrow CAMELYON16) and cross-center (CAMELYON17-0 to CAMELYON17-4) benchmarks, SFDA-DeP consistently outperforms state-of-the-art SFDA in both classification and localization tasks.

References

- Basak, H., Yin, Z.: Forget more to learn more: Domain-specific feature unlearning for semi-supervised and unsupervised domain adaptation. In: ECCV (2024) 4
- Belharbi, S., Pedersoli, M., Ben Ayed, I., McCaffrey, L., Granger, E.: Negative evidence matters in interpretable histology image classification. In: MIDL (2022) 3

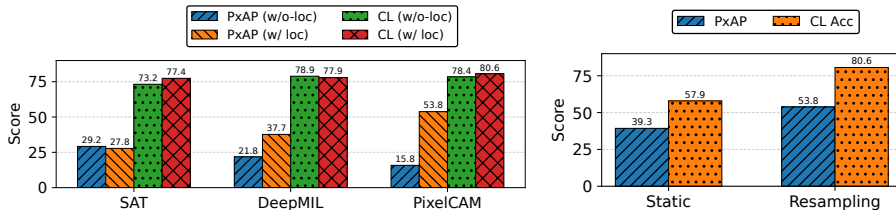


Fig. 3. Impact on performance of (a) the localization loss during adaptation, and of (b) dynamic resampling versus static. (GlaS \rightarrow CAMELYON17).

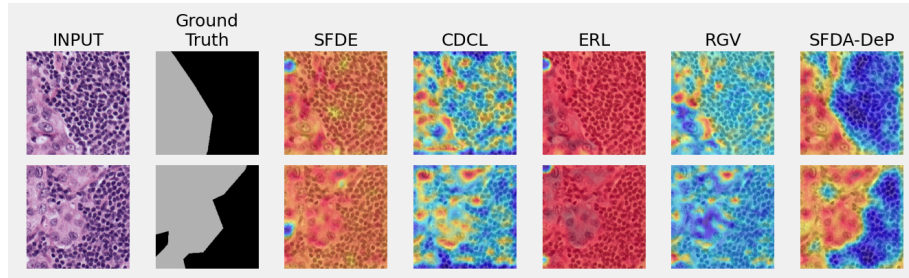


Fig. 4. Activation maps produced by the PixelCAM WSOL model after SFDA-EeP and state-of-the-art SFDA methods (GlaS → CAMELYON17-3).

3. Belharbi, S., Sarraf, A., Pedersoli, M., Ayed, I.B., McCaffrey, L., Granger, E.: F-CAM: Full resolution class activation maps via guided parametric upscaling. In: WACV (2022) 3
4. Chen, H.L., Lu, C.S., Chung, P.C.: Sgcd: Stain-guided cyclediffusion for unsupervised domain adaptation of histopathology image classification. In: NeurIPS (2025) 2
5. Ding, N., Xu, Y., Tang, Y., Xu, C., Wang, Y., Tao, D.: Source-free domain adaptation via distribution estimation. In: CVPR (2022) 4, 7
6. Dosovitskiy, A., Beyer, L., Kolesnikov, A., Weissenborn, D., Zhai, X., Unterthiner, T., Dehghani, M., Minderer, M., Heigold, G., Gelly, S., Uszkoreit, J., Houlsby, N.: An image is worth 16x16 words: Transformers for image recognition at scale. In: ICLR (2021) 6
7. Ehteshami Bejnordi, B., Veta, M., Johannes van Diest, P., et al.: Diagnostic Assessment of Deep Learning Algorithms for Detection of Lymph Node Metastases in Women With Breast Cancer . JAMA (2017) 6
8. Fang, Y., Yap, P.T., Lin, W., Zhu, H., Liu, M.: Source-free unsupervised domain adaptation: A survey. Neural Network (2024) 3
9. Gao, W., Wan, F., Pan, X., Peng, Z., Tian, Q., Han, Z., Zhou, B., Ye, Q.: TS-CAM: token semantic coupled attention map for weakly supervised object localization. In: ICCV (2021) 3
10. Guichemerre, A., Belharbi, S., Mayet, T., Murtaza, S., Shamsolmoali, P., McCaffrey, L., Granger, E.: Source-free domain adaptation of weakly-supervised object localization models for histology. In: CVPRw (2024) 2, 3, 4, 6
11. Guichemerre, A., Belharbi, S., Shateri, M., McCaffrey, L., Granger, E.: Pixelcam: Pixel class activation mapping for histology image classification and roi localization. In: MIDL (2025) 2, 3, 6
12. Ilse, M., Tomczak, J.M., Welling, M.: Attention-based deep multiple instance learning. In: ICML (2018) 3, 6
13. Jiang, P.T., Zhang, C.B., Hou, Q., Cheng, M.M., Wei, Y.: Layercam: Exploring hierarchical class activation maps for localization. TMI 30, 5875–5888 (2021) 3
14. Karimian, B., Avanzato, G., Belharbi, S., Guichemerre, A., McCaffrey, L., Shateri, M., Granger, E.: Clip-it: Clip-based pairing for histology images classification. In: WACV (2026) 2
15. Kawamura, K., Goto, Y., Yanagi, R., Kataoka, H., Irie, G.: Approximate domain unlearning for vision-language models. In: NeurIPS (2025) 4

16. Li, J., Yu, Z., Du, Z., Zhu, L., Shen, H.T.: A comprehensive survey on source-free domain adaptation. *IEEE TPAMI* (2024) [3](#)
17. Liang, J., Hu, D., Feng, J.: Do we really need to access the source data? source hypothesis transfer for unsupervised domain adaptation. *ICML* (2020) [3](#), [4](#)
18. Murtaza, S., Belharbi, S., Pedersoli, M., Sarraf, A., Granger, E.: Dips: Discriminative pseudo-label sampling with self-supervised transformers for weakly supervised object localization. *IMAVIS* (2023) [2](#)
19. Nehdi, T.M., Mrabah, N., Belal, A., Pedersoli, M., Granger, E.: Low-rank expert merging for multi-source domain adaptation in person re-identification. In: *WACV* (2026) [2](#)
20. Rony, J., Belharbi, S., Dolz, J., Ben Ayed, I., McCaffrey, L., Granger, E.: Deep weakly-supervised learning methods for classification and localization in histology images: A survey. *MLBI* **2** (2023) [2](#), [3](#), [6](#), [7](#)
21. Sharafi, M., Belharbi, S., Salem, H.B., Etemad, A., Koerich, A.L., Pedersoli, M., Bacon, S., Granger, E.: Personalized feature translation for expression recognition: An efficient source-free domain adaptation method. In: *ICLR* (2026) [3](#)
22. Sharafi, M., Ollivier, E., Zeeshan, O., Belharbi, S., Koerich, A., Pedersoli, M., Bacon, S., Granger, E.: Disentangled source-free personalization for facial expression recognition with neutral target data. In: *FG* (2025) [2](#)
23. Sirinukunwattana, K., Snead, D., Rajpoot, N.: A stochastic polygons model for glandular structures in colon histology images. *TMI* (2015) [6](#)
24. Wang, R., Wu, Z., Weng, Z., Chen, J., Qi, G.J., Jiang, Y.G.: Cross-domain contrastive learning for unsupervised domain adaptation. *IEEE TMM* (2022) [7](#)
25. Wu, J., Ji, F., Peng, L., Yang, J.: Machine unlearning for alleviating negative transfer in partial-set source-free unsupervised domain adaptation (2024) [3](#), [4](#)
26. Wu, P., Zhai, W., Cao, Y., Luo, J., Zha, Z.J.: Spatial-aware token for weakly supervised object localization. In: *ICCV* (2023) [3](#), [6](#)
27. Xu, G., Guo, H., Yi, L., Ling, C., Wang, B., Yi, G.: Revisiting source-free domain adaptation: a new perspective via uncertainty control. In: *ICLR* (2025) [7](#)
28. Yang, J., Li, P., Yun, X., Zhong, X., Wu, D.: Machine unlearning for source-free unsupervised partial-domain adaptation in remote sensing. *IEEE TGRS* (2025) [3](#), [4](#)
29. Yao, H., Choi, C., Cao, B., Lee, Y., Koh, P.W., Finn, C.: Wild-time: A benchmark of in-the-wild distribution shift over time. In: *NeurIPS Datasets and Benchmarks Track* (2022) [6](#)
30. Yi, L., Xu, G., Xu, P., Li, J., Pu, R., Ling, C., McLeod, A.I., Wang, B.: When source-free domain adaptation meets learning with noisy labels. In: *ICLR* (2023) [7](#)
31. Zeeshan, M.O., Gillet, N., Koerich, A.L., Pedersoli, M., Bremond, F., Granger, E.: Musaco: Multimodal subject-specific selection and adaptation for expression recognition with co-training. In: *WACV* (2026) [2](#)